

## Supporting Information

### A Colloid Chemistry Route for the Preparation of Hierarchically Ordered Mesoporous Layered Double Hydroxides Using Surfactants as Sacrificial Templates

Gábor Varga,<sup>†</sup> Zoltán Somosi,<sup>§</sup> Zoltán Kónya,<sup>#,||</sup> Ákos Kukovecz,<sup>||</sup> István Pálunkó,<sup>†</sup> and Istvan Szilagyi<sup>§,\*</sup>

<sup>†</sup>Materials and Solution Structure Research Group, Department of Organic Chemistry, University of Szeged, H-6720 Szeged, Hungary

<sup>§</sup>MTA-SZTE Lendület Biocolloids Research Group, Interdisciplinary Excellence Center, Department of Physical Chemistry and Materials Science, University of Szeged, H-6720 Szeged, Hungary

<sup>#</sup>MTA-SZTE Reaction Kinetics and Surface Chemistry Research Group, H-6720 Szeged, Hungary

<sup>||</sup>Department of Applied and Environmental Chemistry, University of Szeged, H-6720 Szeged, Hungary

---

**Materials.** Magnesium(II) nitrate hexahydrate ( $Mg(NO_3)_2 \times 6H_2O$ ), aluminum(III) nitrate nonahydrate ( $Al(NO_3)_3 \times 9H_2O$ ), sodium hydroxide (NaOH) stock aqueous solution, sodium dodecyl sulphate (SDS), 96 m/m% ethanol (EtOH), potassium dichromate ( $K_2Cr_2O_7$ ), 25 m/m% ammonia aqueous solution ( $NH_4OH$ ), sodium nitrate ( $NaNO_3$ ) and sodium chloride ( $NaCl$ ) were all purchased from Sigma-Aldrich in analytical purity and were used as received. Purified water was produced by reverse osmosis and UV irradiation processes by a Puranity TU 3+ UV/UF system (VWR).

**Calculation of Surface Charge Density.** The electrophoretic mobilities ( $u$ ) were converted to zeta potentials ( $\zeta$ ) by Smoluchowski's equation as (S1):<sup>1</sup>

$$\zeta = \frac{u\eta}{\epsilon_0 \epsilon} \quad S1$$

where  $\epsilon$  is the relative permittivity of water,  $\epsilon_0$  is the permittivity of vacuum and  $\eta$  is the viscosity of the solvent. To determine the surface charge density ( $\sigma$ ), the Debye-Hückel equation was used:<sup>2</sup>

$$\sigma = \epsilon_0 \epsilon \kappa \Psi_D \quad S2$$

where  $\Psi_D$  is the diffuse layer potential and  $\kappa$  is the inverse Debye length, which can be calculated from the ionic strength. A typical fit is shown in Figure S1.

**Determination of Hydrodynamic Size and Colloidal Stability.** In the dynamic light scattering (DLS) measurements the fluctuating intensity of the scattered light was correlated with the intensity autocorrelation function to obtain the translational diffusion coefficient ( $D_t$ ), which was used to calculate the hydrodynamic radius ( $R_h$ ) of the particles using the Stokes-Einstein equation:<sup>3</sup>

$$R_h = \frac{k_B T}{6\pi\eta D_t}$$

S3

where  $k_B$  is the Boltzmann constant,  $T$  is the absolute temperature.

Time-resolved DLS measurements were used to follow the aggregation processes in the dispersions, in which the  $R_h$  versus time plots were recorded at different experimental conditions (see some examples in Figure S2). Upon aggregation,  $R_h$  data increase linearly with time ( $t$ ) and the apparent aggregation rate constant ( $k_{app}$ ) can be calculated as:<sup>4</sup>

$$\frac{1}{R_h^0} \frac{dR_h(t)}{dt} \Big|_{t \rightarrow 0} = k_{app} \quad S4$$

where  $R_h^0$  is the hydrodynamic radius of the primary particle.

The colloid stability of the samples was expressed in terms of stability ratio ( $W$ ), which by definition is:<sup>4</sup>

$$W = \frac{k_{app}^{\text{fast}}}{k_{app}} \quad S5$$

where “fast” refers to diffusion-controlled aggregation, which can occur at high ionic strength. The equation shows that stability ratio value of one indicates rapid particle aggregation and unstable dispersions, while higher values refer to more stable samples and rather slower aggregation rates.

**Determination of Interlayer Distance.** The distance of one layer together with the interlayer distance was calculated by Bragg’s law:<sup>5</sup>

$$n\lambda = 2d_{hkl}\sin\theta \quad S6$$

where  $n$  is an integer;  $\lambda$  is the wavelength of the incident light,  $d_{hkl}$  is the lattice spacing and  $\Theta$  is the angle of incidence.

**Sorption Capacity.** The adsorbed amount of contaminants was defined in the equilibrium by the following formula:

$$q_e = \frac{(c_0 - c_e)V}{m} \quad S7$$

where  $c_0$  is the initial concentration of anion in solution,  $c_e$  is the equilibrium concentration,  $q_e$  is the equilibrium sorption capacity,  $m$  is the mass of adsorbent and  $V$  is the volume of the solution.

**Langmuir Model:** The maximum adsorbed amount of contaminants was determined by Langmuir equation:<sup>6</sup>

$$\frac{c_e}{q_e} = \left( \frac{1}{K_L} q_m \right) + \left( \frac{c_e}{q_m} \right) \quad S8$$

where  $q_m$  is the theoretical maximum monolayer sorption capacity and  $K_L$  is the Langmuir sorption constant.

**Freundlich Model:** The adsorption isotherms were also analysed by the Freundlich equation as:<sup>7</sup>

$$\ln q_e = \ln K_F + \left( \frac{1}{n} \right) \times \ln c_e \quad S9$$

where  $K_F$  is the Freundlich constant and  $1/n$  is the heterogeneity factor.

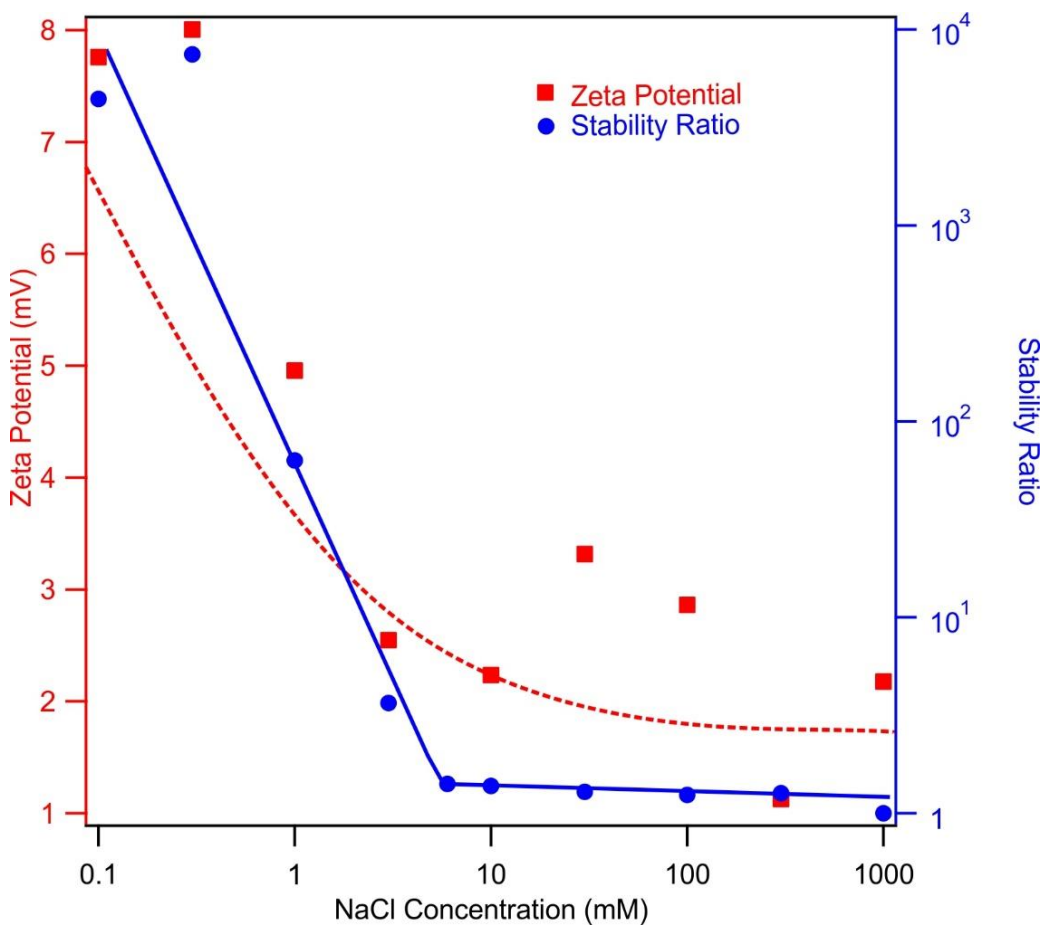


**Figure S1.** Zeta potential (squares) and stability ratio (circles) values of MgAl–Cl–LDH particles versus NaCl concentration. The particle concentration was 10 mg/L. The solid line serves to guide the eyes and the dashed line is the result of calculation using equation S2.

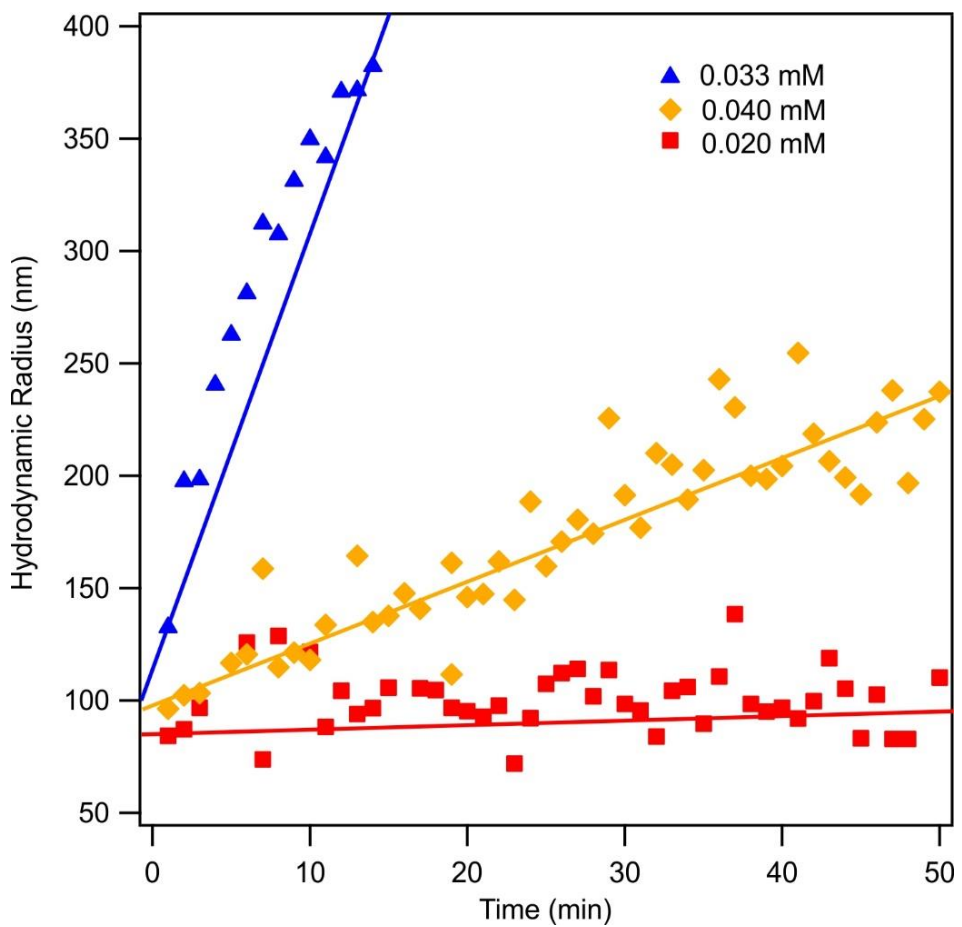


**Figure S2.** Time dependent hydrodynamic radius data at three different SDS concentrations (0.02 mM (red squares), 0.033 mM (blue triangles) and 0.04 mM (yellow diamond)). The particle concentration was set at 10 mg/L and the solid lines are linear fits used for equations S4.

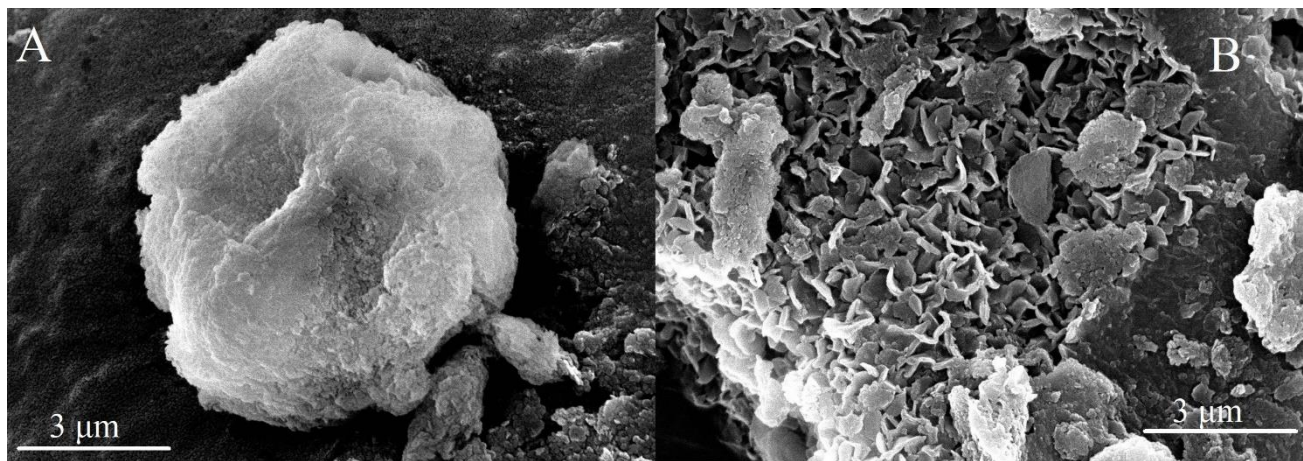


**Figure S3.** SEM images of (A) SDS<sub>30</sub>-MgAl-Cl-LDH and (B) LDH<sub>30</sub> materials.

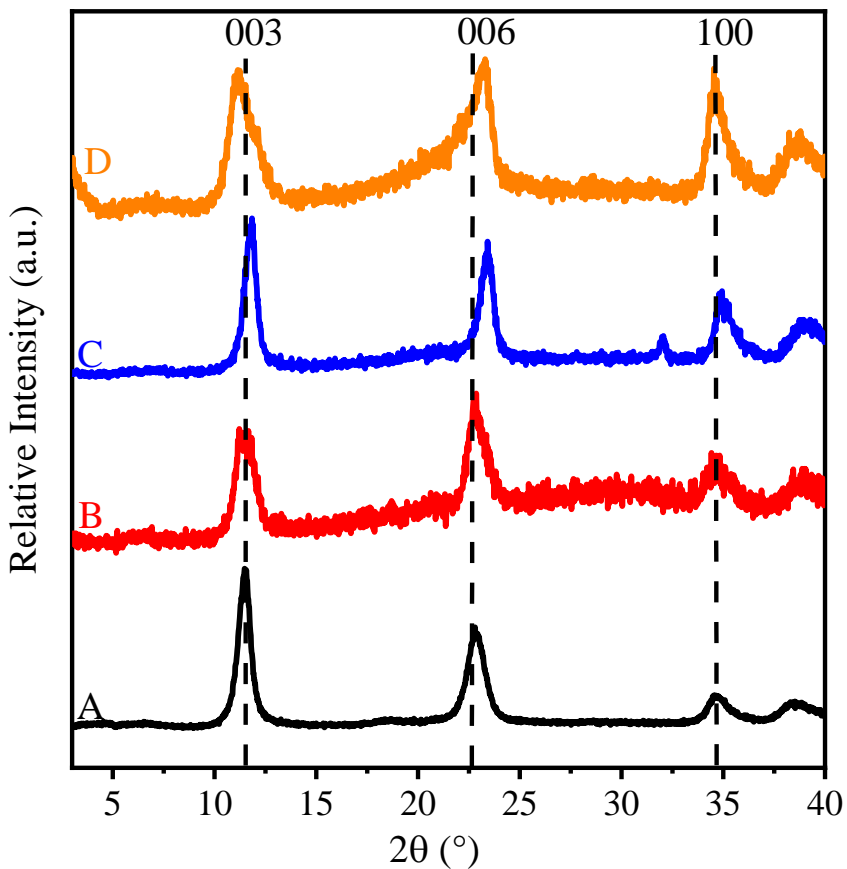


**Figure S4.** XRD patterns of (A) MgAl–Cl–LDH, (B) c-SDS<sub>3</sub>-MgAl–Cl–LDH, (C) c-SDS<sub>10</sub>-MgAl–Cl–LDH and (D) c-SDS<sub>30</sub>-MgAl–Cl–LDH composites prepared by Method 2.

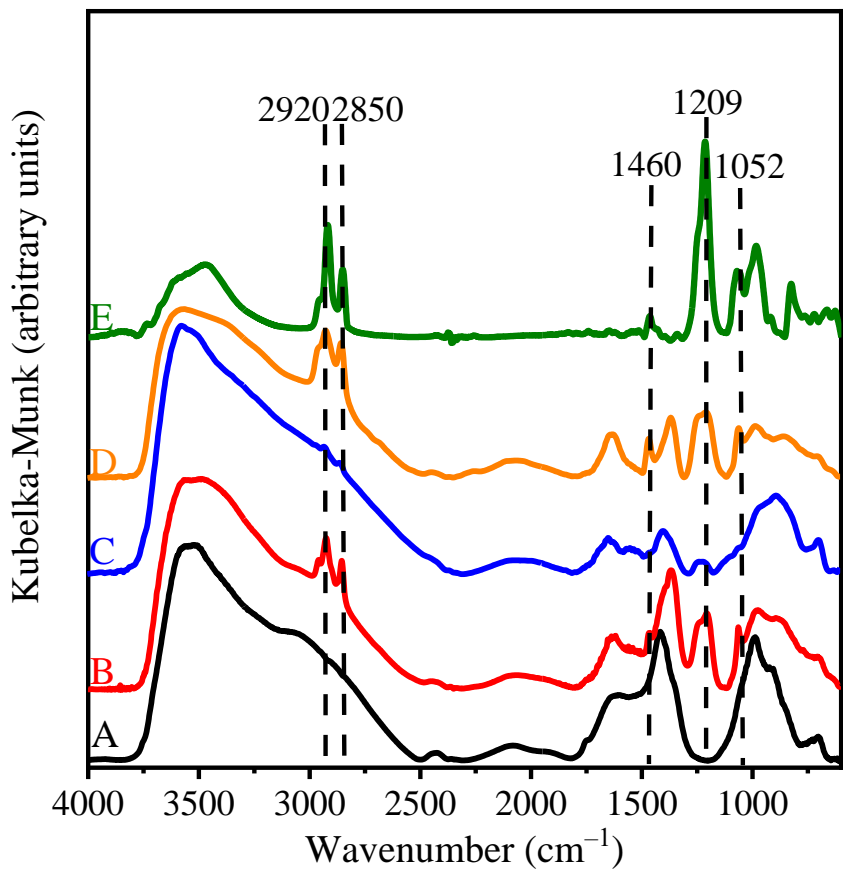


**Figure S5.** IR-DRS spectra of (A) MgAl–Cl–LDH, (B) c-SDS<sub>3</sub>-MgAl–Cl–LDH, (C) c-SDS<sub>10</sub>-MgAl–Cl–LDH, (D) c-SDS<sub>30</sub>-MgAl–Cl–LDH and (E) SDS.

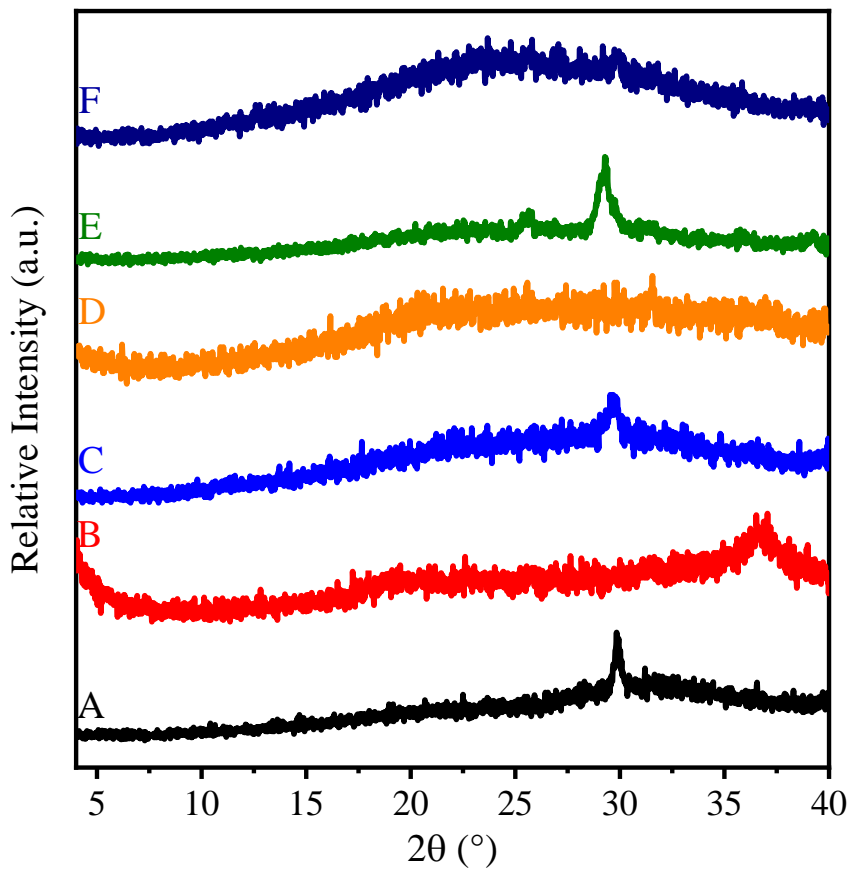


**Figure S6.** XRD patterns of (A)  $\text{LDO}_3$ , (B)  $\text{LDO}_{10}$  and (C)  $\text{LDO}_{30}$  prepared in Method 1 by calcination of  $\text{SDS}_3\text{-MgAl-Cl-LDH}$ ,  $\text{SDS}_{10}\text{-MgAl-Cl-LDH}$  and  $\text{SDS}_{30}\text{-MgAl-Cl-LDH}$ , respectively. XRD patterns of (D) c- $\text{LDO}_3$ , (E) c- $\text{LDO}_{10}$  and (F) c- $\text{LDO}_{30}$  prepared in Method 2 by calcination of c- $\text{SDS}_3\text{-MgAl-Cl-LDH}$ , c- $\text{SDS}_{10}\text{-MgAl-Cl-LDH}$  and c- $\text{SDS}_{30}\text{-MgAl-Cl-LDH}$ , respectively.

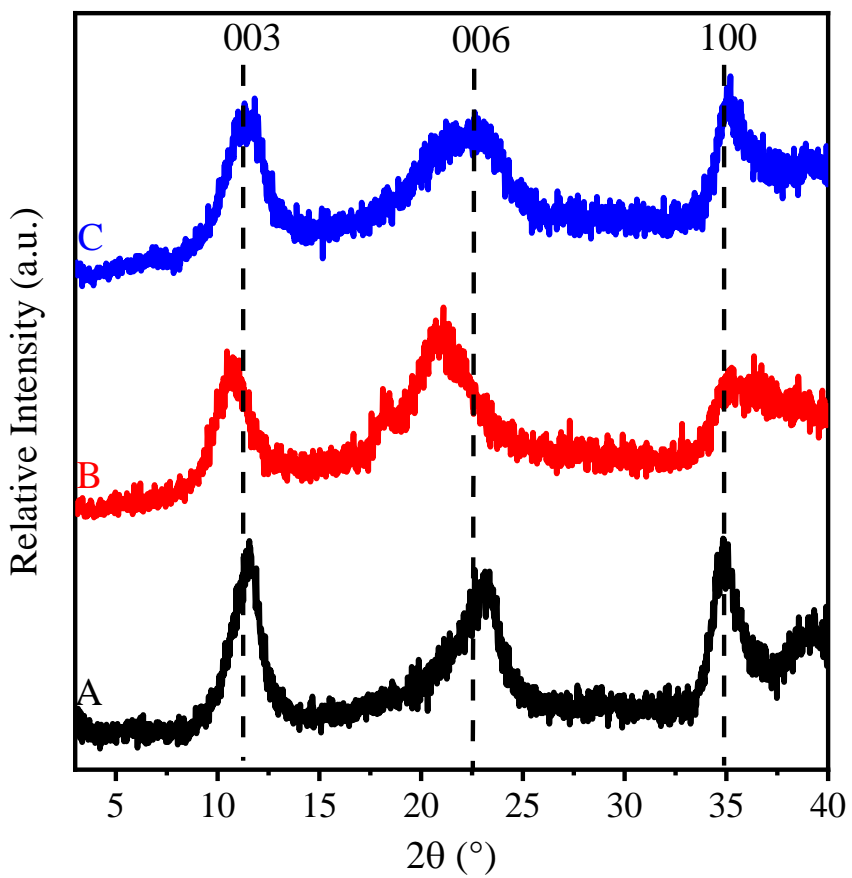


**Figure S7.** XRD patterns of (A) c-LDH<sub>3</sub>, (B) c-LDH<sub>10</sub> and (C) c-LDH<sub>30</sub> obtained after rehydration of LDO<sub>3</sub>, LDO<sub>10</sub> and LDO<sub>30</sub>, respectively in Method 2.

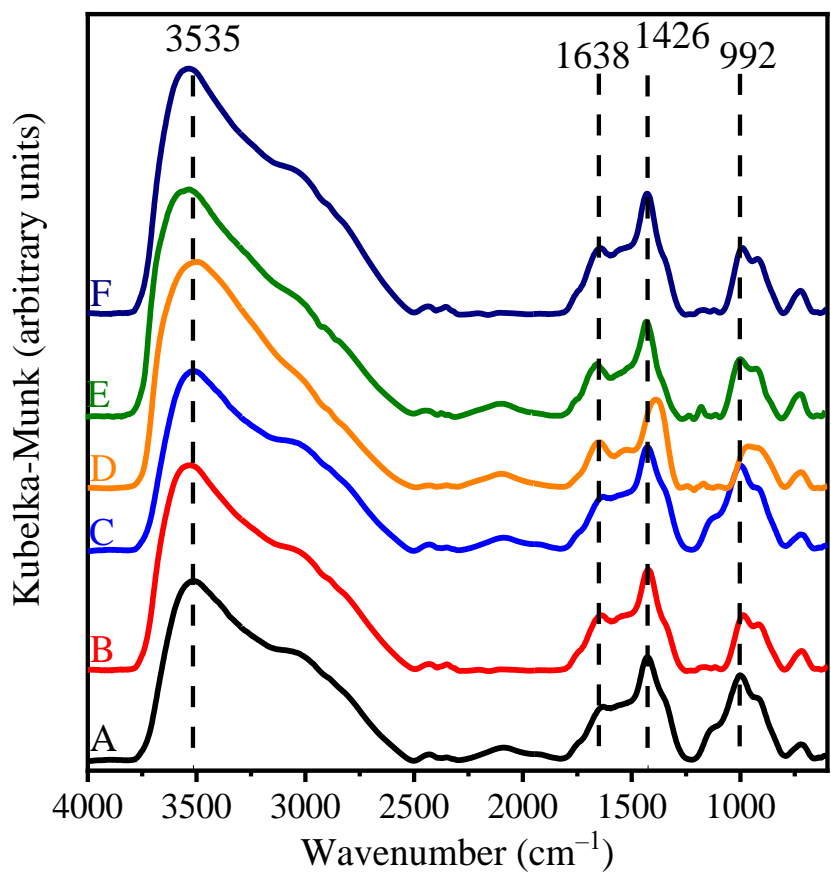


**Figure S8.** IR-DRS spectra of (A)  $\text{LDH}_3$ , (B)  $\text{LDH}_{10}$  and (C)  $\text{LDH}_{30}$ , (D) c- $\text{LDH}_3$ , (E) c- $\text{LDH}_{10}$  and (F) c- $\text{LDH}_{30}$ .

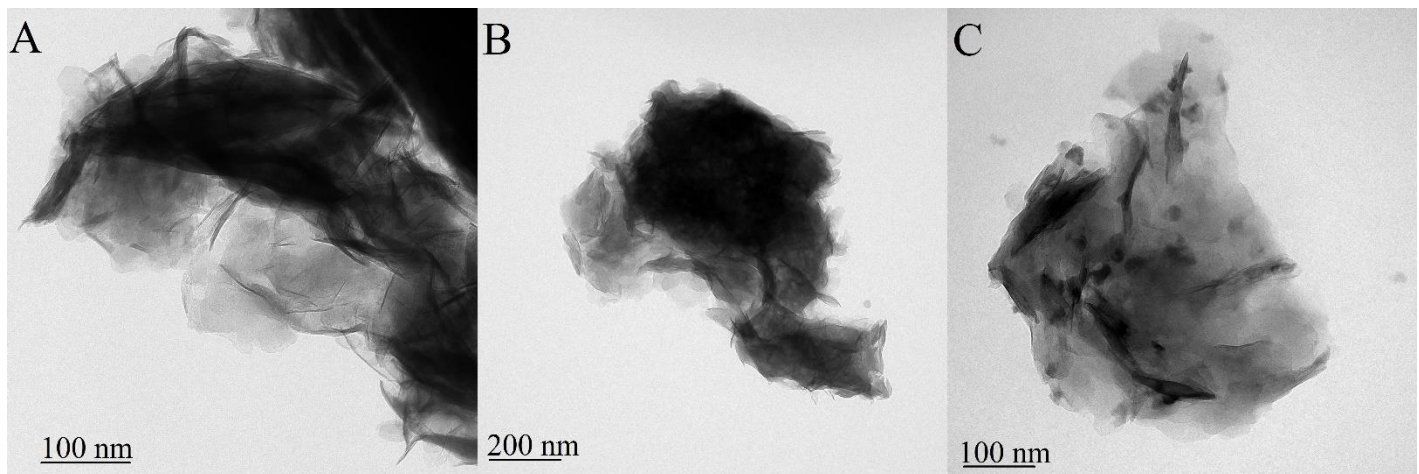


**Figure S9.** TEM images of (A) c-LDH<sub>3</sub>, (B) c-LDH<sub>10</sub> and (C) c-LDH<sub>30</sub> prepared by Method 2.

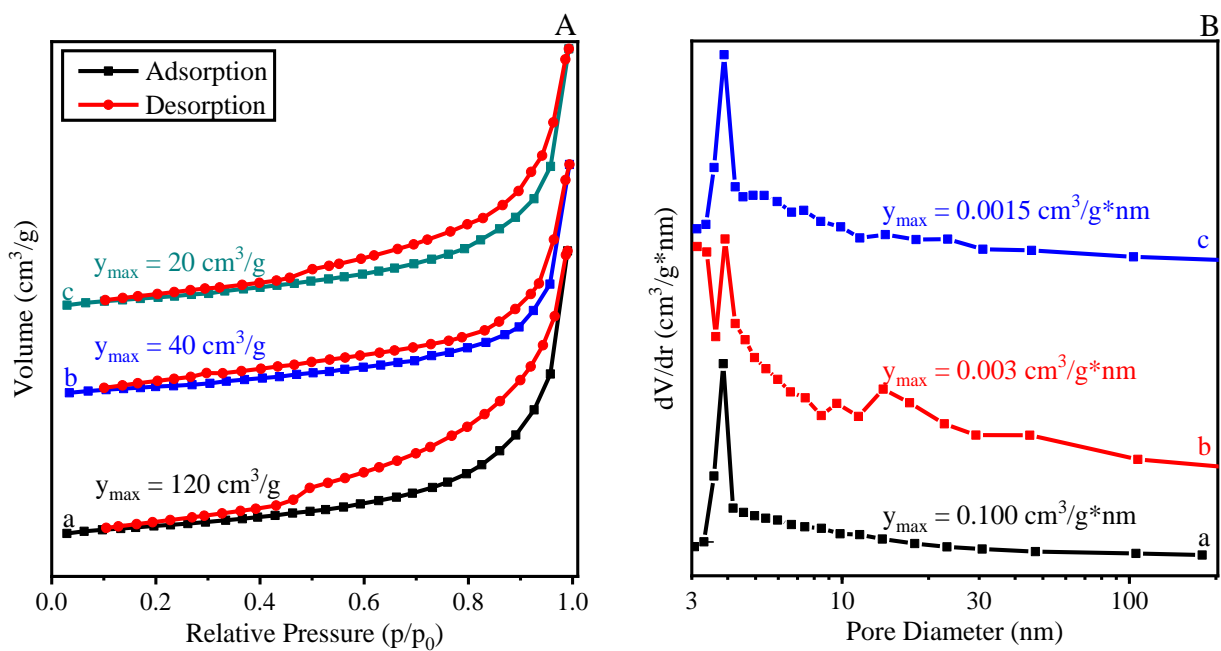


**Figure S10.**  $\text{N}_2$  sorption isotherms (A) and pore diameter distributions (B) of (a) c-LDH<sub>3</sub>, (b) c-LDH<sub>10</sub> and c-LDH<sub>30</sub> prepared by Method 2.

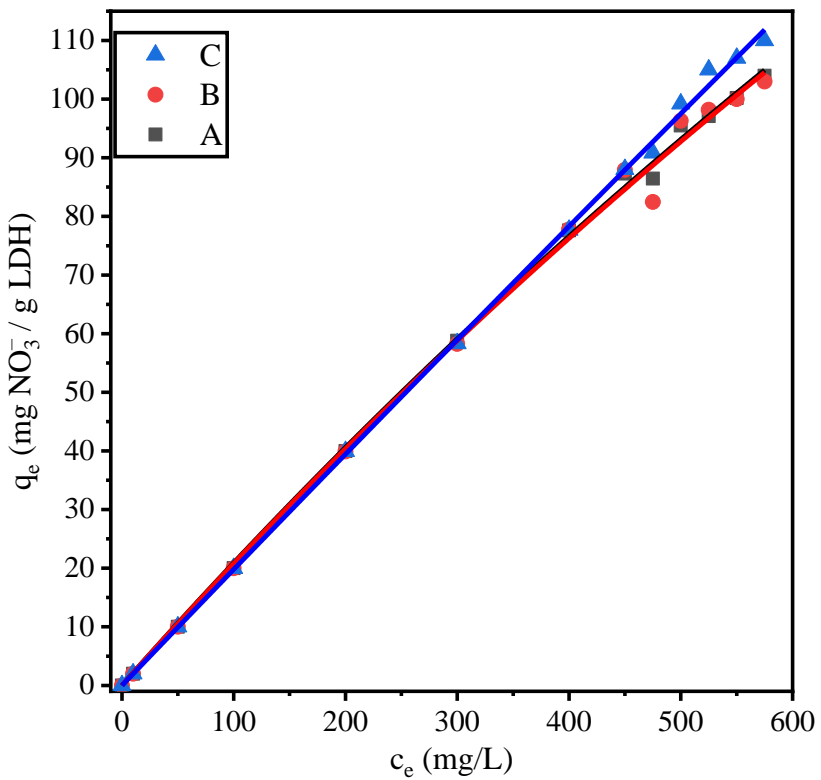


**Figure S11.** Nitrate ion adsorption isotherm of (A)  $\text{LDH}_3$ , (B)  $\text{LDH}_{10}$  and (C)  $\text{LDH}_{30}$  prepared by Method 1. The solid lines indicate the calculations using the Langmuir method (equation S8).

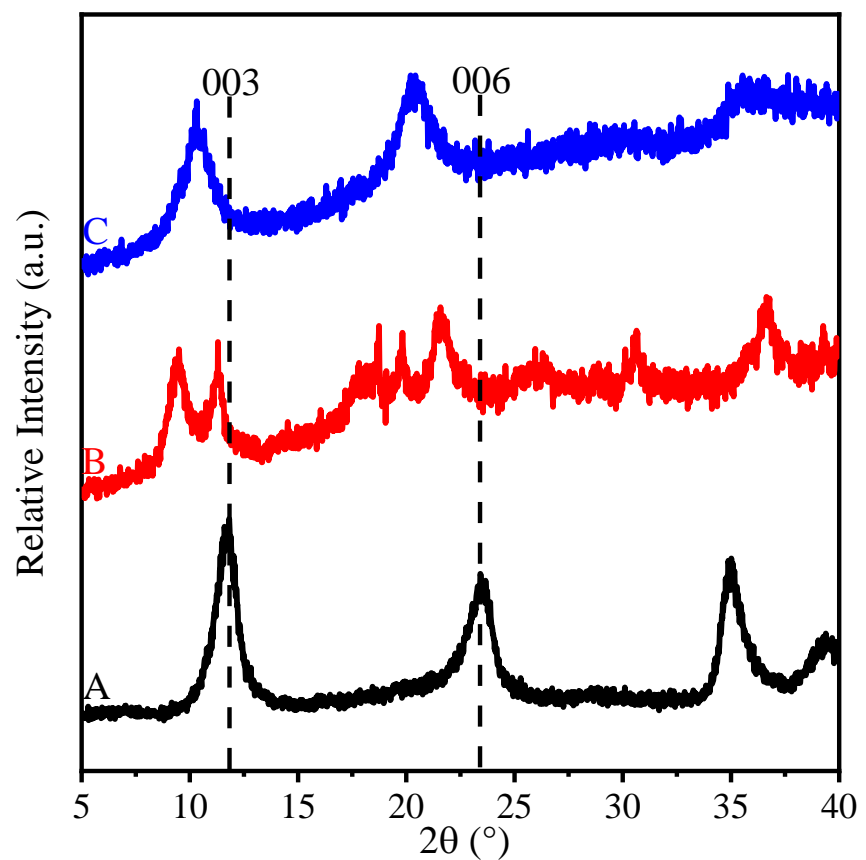


**Figure S12.** XRD patterns of LDH<sub>30</sub> prepared by Method 1 after nitrate adsorption experiments (nitrate concentrations were A: 0 mg/L, B: 200 mg/L and C: 400 mg/L).

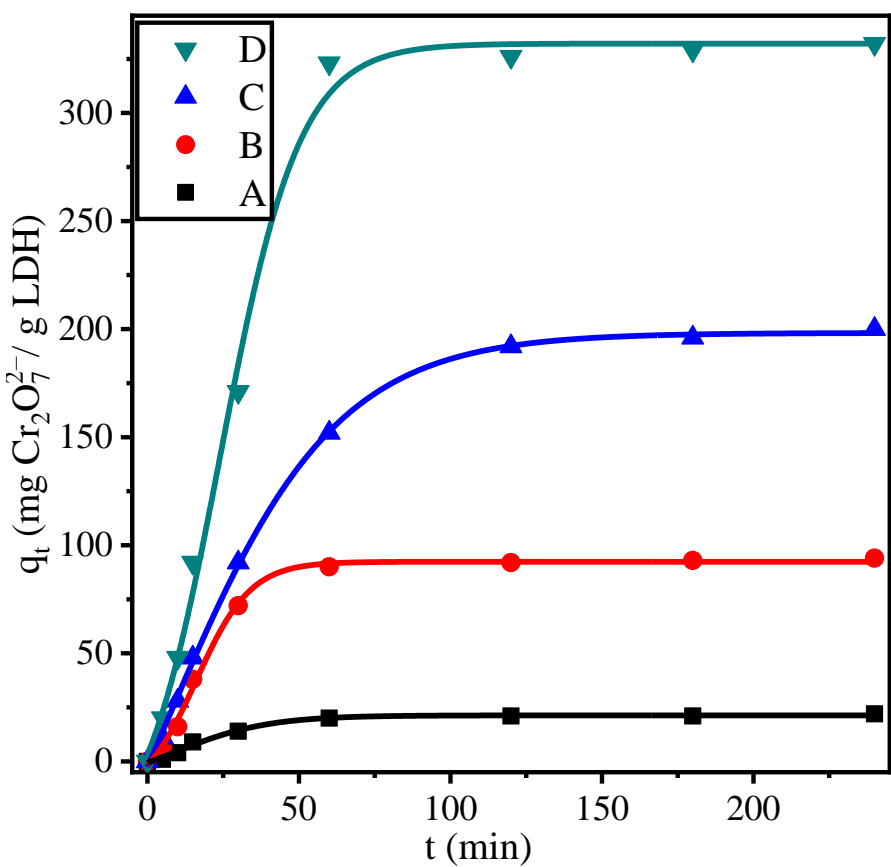


**Figure S13.** Dichromate ion adsorption capacity of (A) MgAl-Cl-LDH, (B) LDH<sub>3</sub>, (C) LDH<sub>10</sub> and (D) LDH<sub>30</sub>. The concentration of dichromate was 1100 mg/L.

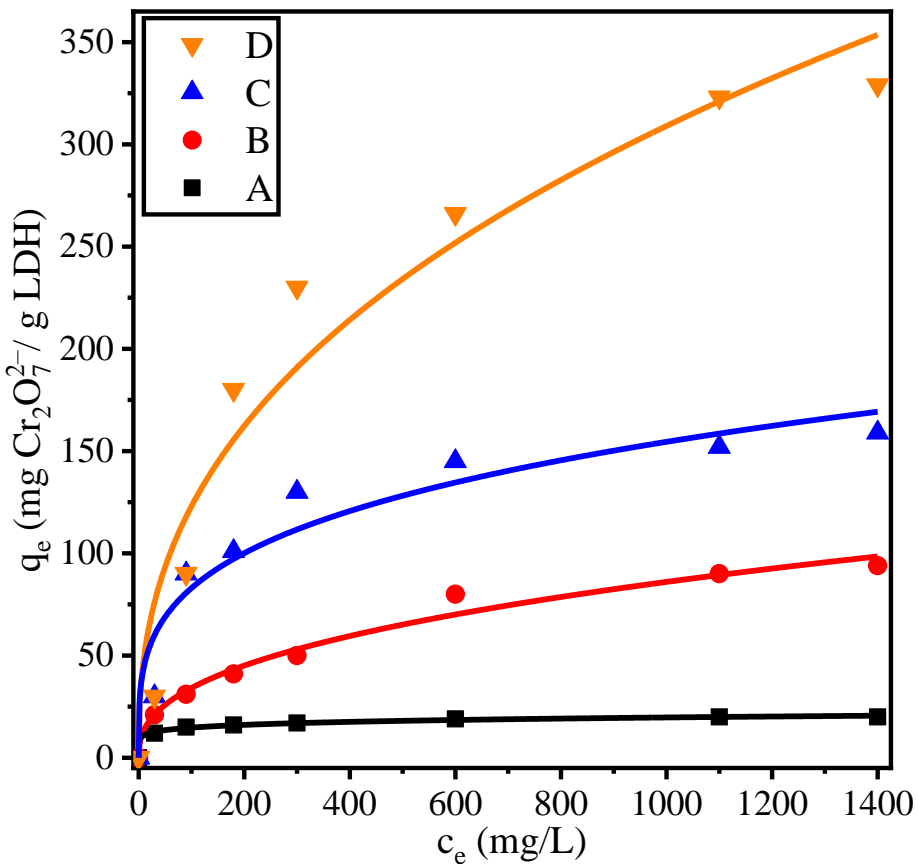


**Figure S14.** Dichromate ion adsorption isotherm of (A) MgAl-Cl-LDH, (B) LDH<sub>3</sub>, (C) LDH<sub>10</sub> and (D) LDH<sub>30</sub>. The solid lines are the fits by the Freundlich isotherm (equation S9).

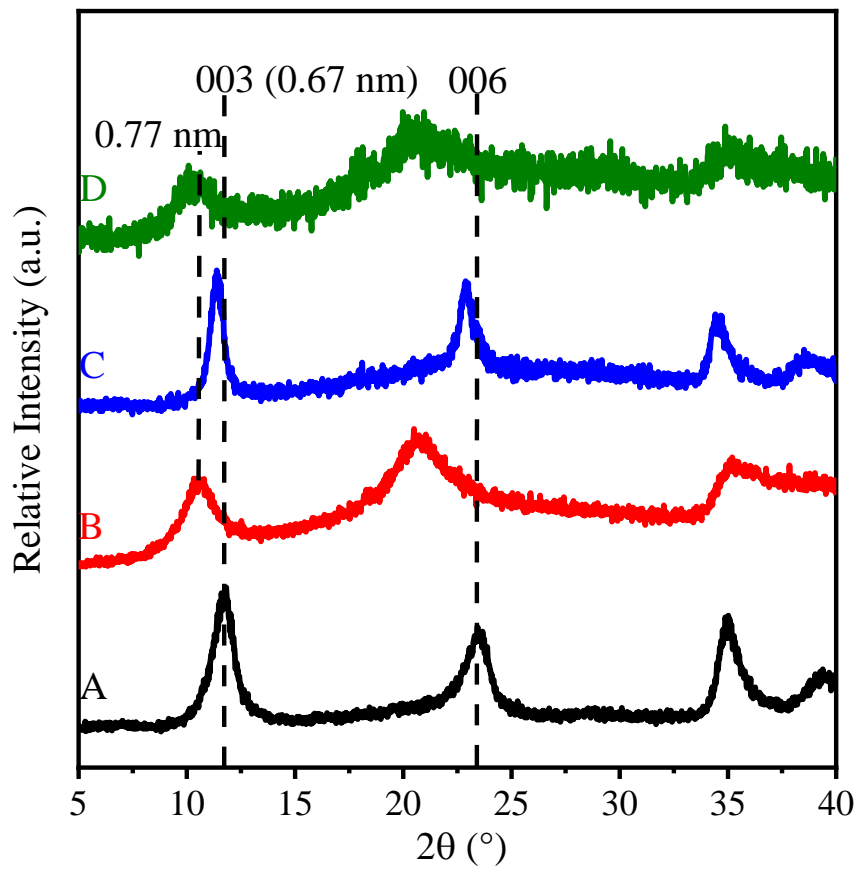


**Figure S15.** XRD patterns of (A) as-prepared LDH<sub>30</sub>, (B) LDH<sub>30</sub> after second use, (C) regenerated LDH<sub>30</sub> after second use and (D) LDH<sub>30</sub> after the fifth reaction cycle.

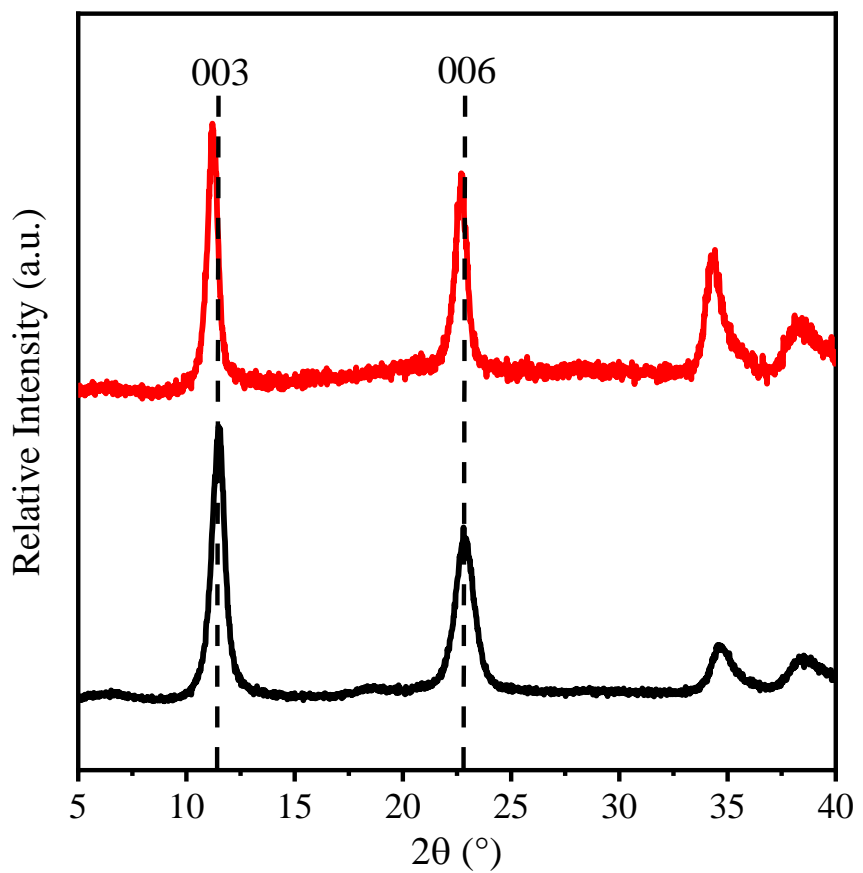


**Figure S16.** XRD patterns of (A) MgAl-Cl-LDH and (B) MgAl-Cl-LDH after ion exchange reaction in dichromate solution.

**Table S1.** Assignments of characteristic IR peaks identified in the pristine and SDS-modified materials prepared by Methods 1 and 2.

Appearance ( $\text{cm}^{-1}$ )	Assignment	Component	Reference
3600-3000	H-bonded $\nu(\text{OH})$	water in LDH-SDS	8-11
2920, 2850	$\nu_{\text{as}}, \nu_{\text{sym}}(\text{CH})$	DS in/on LDH	10,11
1630-1650	$\beta(\text{OH})$	water in LDH	8,9
1470-1460	$\delta(\text{CH})$	DS in/on LDH	9,11
1380-1370			
1420-1410	$\nu_3(\text{CO}_3^{2-})$	surface adsorbed $\text{CO}_3^{2-}$	12
1225-1210	$\nu_{\text{as}}(\text{S=O})$	DS in/on LDH	10,11
1060	$\nu_{\text{sym}}(\text{S=O})$	DS in/on LDH	10,11
1000-990	$\nu_2(\text{CO}_3^{2-})$	surface adsorbed $\text{CO}_3^{2-}$	12

$\nu(\text{OH})$  – stretching mode vibration of –OH group;  $\nu_{\text{as}}, \nu_{\text{sym}}$  (CH) – asymmetric and symmetric stretching mode vibrations of alkyl –CH group;  $\beta(\text{OH})$  – bending mode vibration of –OH group;  $\delta(\text{CH})$  – bending mode vibration of alkyl –CH group;  $\nu_{\text{as}}, \nu_{\text{sym}}$  (S=O) – asymmetric and symmetric stretching mode vibrations of –S=O group and  $\nu_2, \nu_3$  ( $\text{CO}_3^{2-}$ ) – asymmetric deformation and asymmetric stretching mode vibrations of carbonate ions.

**Table S2.** Structural data of the LDH materials synthesized by Method 1 or Method 2.

Composites	Method	Main mesopore diameter (nm) <sup>a</sup>	Other mesopore diameter (nm) <sup>a</sup>	Specific surface (BET) area (m <sup>2</sup> /g) <sup>a</sup>	Total pore volume (cm <sup>3</sup> /g) <sup>a</sup>
LDH	2 <sup>b</sup>	—	—	50	0.0054
LDH <sub>3</sub>	1	3.5	—	30	0.1309
LDH <sub>10</sub>	1	3.9	4.5-17.8	330	0.2215
LDH <sub>30</sub>	1	3.8	5.2-47.8	400	0.2553
c-LDH <sub>3</sub>	2	3.9	—	180	0.1075
c-LDH <sub>10</sub>	2	—	—	35	0.0327
c-LDH <sub>30</sub>	2	—	—	30	0.0150

<sup>a</sup>Calculated from BET isotherms and pore analysis. <sup>b</sup> Prepared by the same as protocol as Method 2, but no SDS was added during the co-precipitation step.

**Table S3.** Comparative table of specific surface area and pore volume of different MgAl-LDHs.

Synthesis	Template	Specific Surface Area (m <sup>2</sup> /g)	Total pore volume (cm <sup>3</sup> /g)	Reference
<b>Our work (LDH<sub>30</sub>)</b>	SDS	<b>400.0</b>	<b>0.25</b>	—
Co-precipitation method + (AMOST)	—	263.0	1.07	13
Surface templated method	SDS	213.6	—	14
Grown on electrospun	Polyacrylnitril membrane	238.0	—	15
urea method + hydrothermal treatment	Al(OH) <sub>3</sub>	288.0	0.66	16
Co-precipitation method	—	499.0	0.177	17
Soft template method	SDS	41.2	0.076	18
Hydrothermal method	—	67.5	0.344	19
AMOST	—	507.0	2.078	20
co-precipitation	—	110.6	—	21
Ethylene glycol	—	164.7	—	22
AMOST	—	365.0	—	23
CO <sub>2</sub> supercritical drying	—	305.0	0.974	24
sol-gel method	—	264.0	0.52	25
in situ growth method	SiO <sub>2</sub>	124.7	—	26
Dehydration-rehydration method	CNS	53.9	—	27
epoxide-mediated sol-gel reaction/method	—	293.0	0.49	28
opal inverse method	PS	170.0	—	29
co-precipitation	PS	74.0	—	30
templated impregnation + co-precipitation	PS	42.0	—	31
opal inverse method	PS	170.0	—	32
alkali-free co-precipitation	PS	62.0	0.091	33

AMOST: Aqueous miscible organic solvent treatment; CNS: Carbon nanosphere; PS: Polystyrene.

**Table S4.** Langmuir parameters for adsorption of nitrate ion.

<b>Adsorbent</b>	<b><math>q_m</math> (mg/g)</b>	<b><math>K_L</math> (L/mg)</b>	<b><math>R^2</math></b>
LDH <sub>3</sub>	682.9	0.00031	0.998
LDH <sub>10</sub>	689.2	0.00032	0.996
LDH <sub>30</sub>	749.7	0.00022	0.999

**Table S5.** Nitrate adsorption capacity and BET data of different LDH adsorbers used for nitrate removal.

Material	Synthesis	BET (m <sup>2</sup> /g)	Sorption capacity (mg/g)	Langmuir (L/mg)	Interlayer distance (Å)	Reference
<b>LDH<sub>30</sub></b>	<b>SDS templated co-precipitation</b>	<b>400</b>	<b>749.7</b>	<b>0.00022</b>	<b>6.7</b>	<b>Our work</b>
MgAl–Cl–LDH	co-precipitation	64	118.1	0.088	7.6	34
	co-precipitation					
MgFe–Cl–LDH	+ hydrothermal aging	70	31.2	0.09	7.9	35
MgAl–Cl–LDH	co-precipitation	—	340.0	—	—	36
ZnAl–Cl–LDH	co-precipitation	198	640.0	0.0015	7.3	37
MgAl–Cl–LDH	co-precipitation at low saturation	—	350.0	—	7.8	38
MgAl–CO <sub>3</sub> –LDH	co-precipitation at low saturation	—	450.0	—	7.5	38

**Table S6.** Comparative table of dichromate sorption capacity of different LDH adsorbers.

<b>Material</b>	<b>Synthesis</b>	<b>BET (m<sup>2</sup>/g)</b>	<b>Sorption capacity (mg/g)</b>	<b>Langmuir (L/mg)</b>	<b>Interlayer distance (Å)</b>	<b>Reference</b>
<b>SDS templated</b>						
<b>LDH30</b>	co- precipitation	<b>400</b>	<b>388.8</b>	<b>0.00042</b>	<b>6.7</b>	<b>Our work</b>
MgAl-NO <sub>3</sub> - LDH nanosheets	hydrothermal	65.9	63.9	—	5.8	39
MgAl-LDH (no further info)	in situ	—	339.0	0.004312	7.7	40
MgAl-CO <sub>3</sub> - LDH	co-precipitation	—	246.0	0.000701	7.6	40
MgAl-NO <sub>3</sub> - LDH/Aluminium foams	in-situ growth	—	27.8	0.071	—	41
Graphene-MgAl- LDH nanocomposite	urea hydrolysis – hydrothermal method	34.9	172.5	14.7	7.5	42
MgAl-NO <sub>3</sub> - LDH Nanosheets	Anion exchange and exfoliation	—	125.97	—	4.8	43
MgZnAl- NO <sub>3</sub> - LDH	co-precipitation	51.1	29.3	—	7.8	44
MgZnAl- NO <sub>3</sub> - LDH rehydratated	calcination– rehydration	64.3	33.82	—	—	44
NiAl-NO <sub>3</sub> -LDH	co-precipitation	171.4	373.6	0.00422	7.8	45
NiAl-Glycine- LDH	separate nucleation	61.1	68.4	0.598	13.1	46
CoBi-NO <sub>3</sub> -LDH	urea hydrolysis	70.0	277.7	—	3.1	47
NiFe-LDH microsphere	hydrothermal method	136.0	35.9	0.362	—	48
Graphene Oxid@NiFe- LDH composite	hydrothermal method	145.0	51.7	0.443	—	48

MgAl-NO <sub>3</sub> -LDH	urea hydrolysis -hydrothermal method	17.8	30.3	0.0139	7.6	49
NiAl-NO <sub>3</sub> -LDH	urea hydrolysis -hydrothermal method	53.1	57.5	0.0102	7.6	50
ZnAl-NO <sub>3</sub> -LDH	urea hydrolysis -hydrothermal method	56.1	68.1	0.0101	7.6	51
ZnAl-Cl-LDH	co-precipitation magnetic	—	247.9	1.286	7.8	52
alginate-MgAl LDH	entrapment	73.3	11.2	0.01	—	53
MgAl-Cl-LDH	co-precipitation + Thermal treatment	—	88.1	—	—	54
NiCo-NO <sub>3</sub> -LDH	—	267.0	99.9	0.066	—	55
CoFe <sub>2</sub> O <sub>4</sub> @MgAl -LDH composite	hydrothermal method	120.8	72.4	0.032	—	56
MgAl-CO <sub>3</sub> -LDH	co-precipitation	84.0	17.0	—	—	57
Fe <sub>3</sub> O <sub>4</sub> @C@MgA l-LDH	sol-gel method + urea method	—	192.3	0.216	—	58
MgAlCr(III)- LDH	co-precipitation	102.7	237.8	—	—	59
MgAl-LDH	co-precipitation	68.6	199.4	—	—	59
LDHs@MoS <sub>2</sub>	co-precipitation +hydrothermal	85.5	76.3	—	—	60
ZrMgAl- LDH/ZrZnAl- LDH	co-precipitation	238.0/9 1.0	24.0/29.0	0.43	7.2	61
Porous NiMgAl- LDH/LDO	hydrothermal+ dehydration- rehydration	101.0/1 79.0	52.4/94.3	0.067/0.44 6	8.0	62
Porous MgAl/MnAl/Co	PEO templated co-precipitation	293.0/2 47.0/17 5.0/171	60.0/71.0/72.5/5 .0/35.0	—	7.6	28

AlFeAl/NiAl-		.0/314.					
LDH		0					
Porous MgAl-	Vermiculite						
LDH	templated	—	~25.0	—	7.1	—	63
	hydrothermal						

**Table S7.** Dichromate sorption capacity of LDH<sub>30</sub> with commercially available adsorbents.

Material	BET (m <sup>2</sup> /g)	Sorption capacity (mg/g)	Langmuir (L/mg)	Reference
<b>LDH<sub>30</sub></b>	<b>400</b>	<b>388.8</b>	<b>0.00042</b>	<b>Our work</b>
Chitosan biosorbent	125.2	153.8	0.0023	64
N-Methylimidazolium functionalized strongly basic anion exchange resins	—	132.0	3.8	65
activated carbon (Filtrosorb 400)	1200.0	125.5	4.6	66
sawdust	—	3.3	0.167	67
activated carbon (Filtrosorb 400) (pH = 2.5)	>200.0	145.0	—	68
sphagnum moss peat	—	119.0	0.0022	68
compost	—	101.0	—	68
leather based activated carbon	646.0–2402.0	241.0	—	69
TMU-30 (MOF)	—	145.0	—	70

## References

1. Delgado, A. V.; Gonzalez-Caballero, F.; Hunter, R. J.; Koopal, L. K.; Lyklema, J., Measurement and interpretation of electrokinetic phenomena. *J. Colloid Interface Sci.* **2007**, *309*, 194-224.
2. Trefalt, G.; Szilagyi, I.; Borkovec, M., Poisson-Boltzmann description of interaction forces and aggregation rates involving charged colloidal particles in asymmetric electrolytes. *J. Colloid Interface Sci.* **2013**, *406*, 111-120.
3. Hassan, P. A.; Rana, S.; Verma, G., Making sense of Brownian motion: Colloid characterization by dynamic light scattering. *Langmuir* **2015**, *31*, 3-12.
4. Holthoff, H.; Egelhaaf, S. U.; Borkovec, M.; Schurtenberger, P.; Sticher, H., Coagulation rate measurements of colloidal particles by simultaneous static and dynamic light scattering. *Langmuir* **1996**, *12*, 5541-5549.
5. Bragg, W. H.; Bragg, W. L., The reflection of X-rays by crystals. *Proc. R. soc. Lond. Ser. A-Contain. Pap. Math. Phys. Character* **1913**, *88*, 428-438.
6. Langmuir, I., The adsorption of gases on plane surfaces of glass, mica and platinum. *J. Am. Chem. Soc.* **1918**, *40*, 1361-1403.
7. Freundlich, H., Über die adsorption in lösungen. *Z. Phys. Chem.* **1907**, *57*, 385-470.
8. Rives, V.; Kannan, S., Layered double hydroxides with the hydrotalcite-type structure containing Cu<sup>2+</sup>, Ni<sup>2+</sup> and Al<sup>3+</sup>. *J. Mater. Chem.* **2000**, *10*, 489-495.
9. Iyi, N.; Matsumoto, T.; Kaneko, Y.; Kitamura, K., Deintercalation of carbonate ions from a hydrotalcite-like compound: Enhanced decarbonation using acid-salt mixed solution. *Chem. Mat.* **2004**, *16*, 2926-2932.
10. Sun, Y.; Zhou, Y.; Ye, X.; Chen, J.; Wang, Z., Fabrication and infrared emissivity study of hybrid materials based on immobilization of collagen onto exfoliated LDH. *Mater. Lett.* **2008**, *62*, 2943-2946.
11. Zhang, P.; Qian, G. R.; Xu, Z. P.; Shi, H. S.; Ruan, X. X.; Yang, J.; Frost, R. L., Effective adsorption of sodium dodecylsulfate (SDS) by hydrocalumite (CaAl-LDH-Cl) induced by self-dissolution and re-precipitation mechanism. *J. Colloid Interface Sci.* **2012**, *367*, 264-271.
12. Kloprogge, J. T.; Wharton, D.; Hickey, L.; Frost, R. L., Infrared and Raman study of interlayer anions CO<sub>3</sub><sup>2-</sup>, NO<sub>3</sub><sup>-</sup>, SO<sub>4</sub><sup>2-</sup> and ClO<sub>4</sub><sup>-</sup> in Mg/Al hydrotalcite. *Am. Miner.* **2002**, *87*, 623-629.
13. Wang, Q.; O'Hare, D., Large-scale synthesis of highly dispersed layered double hydroxide powders containing delaminated single layer nanosheets. *Chem. Commun.* **2013**, *49*, 6301-6303.
14. Shao, M. F.; Ning, F. Y.; Zhao, J. W.; Wei, M.; Evans, D. G.; Duan, X., Hierarchical layered double hydroxide microspheres with largely enhanced performance for ethanol electrooxidation. *Adv. Funct. Mater.* **2013**, *23*, 3513-3518.
15. Shami, Z.; Amininasab, S. M.; Shakeri, P., Structure-property relationships of nanosheeted 3D hierarchical roughness MgAl-layered double hydroxide branched to an electrospun porous nanomembrane: A superior oil-removing nanofabric. *ACS Appl. Mater. Interfaces* **2016**, *8*, 28964-28973.
16. Li, J.; Zhang, N.; Ng, D. H. L., Synthesis of a 3D hierarchical structure of gamma-Al(OH)/Mg-Al-LDH/C and its performance in organic dyes and antibiotics adsorption. *J. Mater. Chem. A* **2015**, *3*, 21106-21115.
17. Nijs, H.; De Bock, M.; Vansant, E. F., Evaluation of the microporosity of pillared Fe(CN)(6)-MgAl-LDHs. *Microporous Mesoporous Mat.* **1999**, *30*, 243-253.
18. Zhang, J.; Xie, X. L.; Li, C. J.; Wang, H.; Wang, L. J., The role of soft colloidal templates in the shape evolution of flower-like MgAl-LDH hierarchical microstructures. *RSC Adv.* **2015**, *5*, 29757-29765.
19. Pourfaraj, R.; Fatemi, S. J.; Kazemi, S. Y.; Biparva, P., Synthesis of hexagonal mesoporous MgAl LDH nanoplatelets adsorbent for the effective adsorption of Brilliant Yellow. *J. Colloid Interface Sci.* **2017**, *508*, 65-74.

20. Jia, H. H.; Zhao, Y.; Niu, P. P.; Lu, N. Y.; Fan, B. B.; Li, R. F., Amine-functionalized MgAl LDH nanosheets as efficient solid base catalysts for Knoevenagel condensation. *Mol. Catal.* **2018**, *449*, 31-37.
21. Shou, J. X.; Jiang, C. F.; Wang, F.; Qiu, M. Q.; Xu, Q. G., Fabrication of Fe<sub>3</sub>O<sub>4</sub>/MgAl-layered double hydroxide magnetic composites for the effective decontamination of Co(II) from synthetic wastewater. *J. Mol. Liq.* **2015**, *207*, 216-223.
22. Ni, X. M.; Kuang, K. Q.; Jin, X.; Xiao, X. K.; Liao, G. X., Large scale synthesis of porous microspheres of Mg-Al-layered double hydroxide with improved fire suppression effectiveness. *Solid State Sci.* **2010**, *12*, 546-551.
23. Chen, C. P.; Wangriya, A.; Buffet, J. C.; O'Hare, D., Tuneable ultra high specific surface area Mg/Al-CO<sub>3</sub> layered double hydroxides. *Dalton Trans.* **2015**, *44*, 16392-16398.
24. Touati, S.; Mansouri, H.; Bengueeddach, A.; de Roy, A.; Forano, C.; Prevot, V., Nanostructured layered double hydroxide aerogels with enhanced adsorption properties. *Chem. Commun.* **2012**, *48*, 7197-7199.
25. Tokudome, Y.; Tarutani, N.; Nakanishi, K.; Takahashi, M., Layered double hydroxide (LDH)-based monolith with interconnected hierarchical channels: enhanced sorption affinity for anionic species. *J. Mater. Chem. A* **2013**, *1*, 7702-7708.
26. Shao, M. F.; Ning, F. Y.; Zhao, Y. F.; Zhao, J. W.; Wei, M.; Evans, D. G.; Duan, X., Core-shell layered double hydroxide microspheres with tunable interior architecture for supercapacitors. *Chem. Mat.* **2012**, *24*, 1192-1197.
27. Gunawan, P.; Xu, R., Direct assembly of anisotropic layered double hydroxide (LDH) nanocrystals on spherical template for fabrication of drug-LDH hollow nanospheres. *Chem. Mat.* **2009**, *21*, 781-783.
28. Tarutani, N.; Tokudome, Y.; Fukui, M.; Nakanishi, K.; Takahashi, M., Fabrication of hierarchically porous monolithic layered double hydroxide composites with tunable microcages for effective oxyanion adsorption. *RSC Adv.* **2015**, *5*, 57187-57192.
29. Geraud, E.; Bouhent, M.; Derriche, Z.; Leroux, F.; Prevot, V.; Forano, C., Texture effect of layered double hydroxides on chemisorption of Orange II. *J. Phys. Chem. Solids* **2007**, *68*, 818-823.
30. Geraud, E.; Prevot, V.; Ghanbaja, J.; Leroux, F., Macroscopically ordered hydrotalcite-type materials using self-assembled colloidal crystal template. *Chem. Mat.* **2006**, *18*, 238-240.
31. Geraud, E.; Rafqah, S.; Sarakha, M.; Forano, C.; Prevot, V.; Leroux, F., Three dimensionally ordered macroporous layered double hydroxides: Preparation by templated impregnation/coprecipitation and pattern stability upon calcination. *Chem. Mat.* **2008**, *20*, 1116-1125.
32. Halma, M.; Castro, K.; Prevot, V.; Forano, C.; Wypych, F.; Nakagaki, S., Immobilization of anionic iron(III) porphyrins into ordered macroporous layered double hydroxides and investigation of catalytic activity in oxidation reactions. *J. Mol. Catal. A-Chem.* **2009**, *310*, 42-50.
33. Woodford, J. J.; Dacquin, J. P.; Wilson, K.; Lee, A. F., Better by design: nanoengineered macroporous hydrotalcites for enhanced catalytic biodiesel production. *Energy Environ. Sci.* **2012**, *5*, 6145-6150.
34. Halajnia, A.; Oustan, S.; Najafi, N.; Khataee, A. R.; Lakzian, A., Adsorption-desorption characteristics of nitrate, phosphate and sulfate on Mg-Al layered double hydroxide. *Appl. Clay Sci.* **2013**, *80-81*, 305-312.
35. Sasai, R.; Norimatsu, W.; Matsumoto, Y., Nitrate-ion-selective exchange ability of layered double hydroxide consisting of Mg-II and Fe-II. *J. Hazard. Mater.* **2012**, *215*, 311-314.
36. Torres-Dorante, L. O.; Lammel, J.; Kuhlmann, H.; Witzke, T.; Olfs, H. W., Capacity, selectivity, and reversibility for nitrate exchange of a layered double-hydroxide (LDH) mineral in simulated soil solutions and in soil. *J. Plant Nutr. Soil Sci.* **2008**, *171*, 777-784.
37. Islam, M.; Patel, R., Synthesis and physicochemical characterization of Zn/Al chloride layered double hydroxide and evaluation of its nitrate removal efficiency. *Desalination* **2010**, *256*, 120-128.

38. Ivanova, D.; Albert, P.; Kavulicova, J., Nitrate removal from model aqueous solutions and real water by calcined Mg/Al layered double hydroxides. *Appl. Clay Sci.* **2018**, *152*, 65-72.
39. Li, J.; Cui, H. Z.; Song, X. J.; Zhang, G. S.; Wang, X. Z.; Song, Q.; Wei, N.; Tian, J., Adsorption and intercalation of organic pollutants and heavy metal ions into MgAl-LDHs nanosheets with high capacity. *RSC Adv.* **2016**, *6*, 92402-92410.
40. Chao, H. P.; Wang, Y. C.; Tran, H. N., Removal of hexavalent chromium from groundwater by Mg/Al-layered double hydroxides using characteristics of in-situ synthesis. *Environ. Pollut.* **2018**, *243*, 620-629.
41. He, S.; Zhao, Y. F.; Wei, M.; Evans, D. G.; Duan, X., Fabrication of hierarchical layered double hydroxide framework on aluminum foam as a structured adsorbent for water treatment. *Ind. Eng. Chem. Res.* **2012**, *51*, 285-291.
42. Yuan, X. Y.; Wang, Y. F.; Wang, J.; Zhou, C.; Tang, Q.; Rao, X. B., Calcined graphene/MgAl-layered double hydroxides for enhanced Cr(VI) removal. *Chem. Eng. J.* **2013**, *221*, 204-213.
43. Zhang, B.; Luan, L. Y.; Gao, R. T.; Li, F.; Li, Y. J.; Wu, T., Rapid and effective removal of Cr(VI) from aqueous solution using exfoliated LDH nanosheets. *Colloid Surf. A-Physicochem. Eng. Asp.* **2017**, *520*, 399-408.
44. Eshaq, G.; Rabie, A. M.; Bakr, A. A.; Mady, A. H.; ElMetwally, A. E., Cr(VI) adsorption from aqueous solutions onto Mg-Zn-Al LDH and its corresponding oxide. *Desalin. Water Treat.* **2016**, *57*, 20377-20387.
45. Ruiz-Huerta, E. A.; Varela, A. D.; Gomez-Bernal, J. M.; Castillo, F.; Avalos-Borja, M.; SenGupta, B.; Martinez-Villegas, N., Arsenic contamination in irrigation water, agricultural soil and maize crop from an abandoned smelter site in Matehuala, Mexico. *J. Hazard. Mater.* **2017**, *339*, 330-339.
46. Asiabi, H.; Yamini, Y.; Shamsayei, M., Highly selective and efficient removal of arsenic(V), chromium(VI) and selenium(VI) oxyanions by layered double hydroxide intercalated with zwitterionic glycine. *J. Hazard. Mater.* **2017**, *339*, 239-247.
47. Jaiswal, A.; Mani, R.; Banerjee, S.; Gautam, R. K.; Chattopadhyaya, M. C., Synthesis of novel nano-layered double hydroxide by urea hydrolysis method and their application in removal of chromium(VI) from aqueous solution: Kinetic, thermodynamic and equilibrium studies. *J. Mol. Liq.* **2015**, *202*, 52-61.
48. Zheng, Y. Q.; Cheng, B.; You, W.; Yu, J. G.; Ho, W. K., 3D hierarchical graphene oxide-NiFe LDH composite with enhanced adsorption affinity to Congo red, methyl orange and Cr(VI) ions. *J. Hazard. Mater.* **2019**, *369*, 214-225.
49. Wang, W. W.; Zhou, J. B.; Achari, G.; Yu, J. G.; Cai, W. Q., Cr(VI) removal from aqueous solutions by hydrothermal synthetic layered double hydroxides: Adsorption performance, coexisting anions and regeneration studies. *Colloid Surf. A-Physicochem. Eng. Asp.* **2014**, *457*, 33-40.
50. Zhao, S.; Gao, B. Y.; Yue, Q. Y.; Wang, Y., Effect of Enteromorpha polysaccharides on coagulation performance and kinetics for dye removal. *Colloid Surf. A-Physicochem. Eng. Asp.* **2014**, *456*, 253-260.
51. Xu, H.; Xiao, F.; Wang, D. S.; Ye, C. Q., Survey of treatment process in water treatment plant and the characteristics of flocs formed by two new coagulants. *Colloid Surf. A-Physicochem. Eng. Asp.* **2014**, *456*, 211-221.
52. Ait Bentaleb, K.; El Khattabi, E.; Lakraimi, M.; Benaziz, L.; Sabbar, E.; Berraho, M.; Legrouri, A., Removal of Cr(VI) from wastewater by anionic clays. *J. Mater. Environ. Sci.* **2016**, *7*, 2886-2896.
53. Lee, C. G.; Park, J. A.; Lee, I.; Kang, J. K.; Yoon, S. Y.; Kim, S. B., Preparation of magnetic alginate-layered double hydroxide composite adsorbents and removal of Cr(VI) from aqueous solution. *Water Sci. Technol.-Water Supply* **2013**, *13*, 846-853.
54. Otgonjargal, E.; Nyamsuren, B.; Surenjav, E.; Burmaa, G.; Temuujin, J.; Khasbaatar, D., Removal of chromium from aqueous solution by thermally treated MgAl layered double hydroxide. *Ann. Civil Environ. Eng.* **2017**, *1*, 1-8.

55. Hu, H. J.; Liu, J. Y.; Xu, Z. H.; Zhang, L. Y.; Cheng, B.; Ho, W. K., Hierarchical porous Ni/Co-LDH hollow dodecahedron with excellent adsorption property for Congo red and Cr(VI) ions. *Appl. Surf. Sci.* **2019**, *478*, 981-990.
56. Deng, L.; Shi, Z.; Peng, X. X., Adsorption of Cr(VI) onto a magnetic CoFe<sub>2</sub>O<sub>4</sub>/MgAl-LDH composite and mechanism study. *RSC Adv.* **2015**, *5*, 49791-49801.
57. Lazaridis, N. K.; Pandi, T. A.; Matis, K. A., Chromium(VI) removal from aqueous solutions by Mg-Al-CO<sub>3</sub> hydrotalcite: Sorption-desorption kinetic and equilibrium studies. *Ind. Eng. Chem. Res.* **2004**, *43*, 2209-2215.
58. Zhang, H.; Huang, F.; Liu, D. L.; Shi, P., Highly efficient removal of Cr(VI) from wastewater via adsorption with novel magnetic Fe<sub>3</sub>O<sub>4</sub>@C@MgAl-layered double-hydroxide. *Chin. Chem. Lett.* **2015**, *26*, 1137-1143.
59. Wang, X. J.; Zhu, X. P.; Lan, L. M.; Zuo, H. B., Removal of chromium from laboratory wastewater using preparation-adsorption technology with a Mg/Al/Cr layered compound. *RSC Adv.* **2016**, *6*, 85595-85602.
60. Wang, J.; Wang, P. Y.; Wang, H. H.; Dong, J. F.; Chen, W. Y.; Wang, X. X.; Wang, S. H.; Hayat, T.; Alsaedi, A.; Wang, X. K., Preparation of molybdenum disulfide coated Mg/Al layered double hydroxide composites for efficient removal of chromium(VI). *ACS Sustain. Chem. Eng.* **2017**, *5*, 7165-7174.
61. Das, N. N.; Konar, J.; Mohanta, M. K.; Srivastava, S. C., Adsorption of Cr(VI) and Se(IV) from their aqueous solutions onto Zr<sup>4+</sup>-substituted ZnAl/MgAl-layered double hydroxides: effect of Zr<sup>4+</sup> substitution in the layer. *J. Colloid Interface Sci.* **2004**, *270*, 1-8.
62. Lei, C. S.; Zhu, X. F.; Zhu, B. C.; Jiang, C. J.; Le, Y.; Yu, J. G., Superb adsorption capacity of hierarchical calcined Ni/Mg/Al layered double hydroxides for Congo red and Cr(VI) ions. *J. Hazard. Mater.* **2017**, *321*, 801-811.
63. Tian, W. L.; Kong, X. G.; Jiang, M. H.; Lei, X. D.; Duan, X., Hierarchical layered double hydroxide epitaxially grown on vermiculite for Cr(VI) removal. *Mater. Lett.* **2016**, *175*, 110-113.
64. Boddu, V. M.; Abburi, K.; Talbott, J. L.; Smith, E. D., Removal of hexavalent chromium from wastewater using a new composite chitosan biosorbent. *Environ. Sci. Technol.* **2003**, *37*, 4449-4456.
65. Zhu, L.; Liu, Y.; Chen, J., Synthesis of N-methylimidazolium functionalized strongly basic anion exchange resins for adsorption of Cr(VI). *Ind. Eng. Chem. Res.* **2009**, *48*, 3261-3267.
66. Huang, C. P.; Wu, M. H., Removal of chromium(VI) from dilute aqueous-solution by activated carbon. *Water Res.* **1977**, *11*, 673-679.
67. Srivastava, H. C. P.; Mathur, R. P.; Mehrotra, I., Removal of chromium from industrial effluents by adsorption on sawdust. **1986**, *7*, 55-63.
68. Sharma, D. C.; Forster, C. F., Removal of hexavalent chromium using sphagnum moss peat. *Water Res.* **1993**, *27*, 1201-1208.
69. Perezcandela, M.; Martinmartinez, J. M.; Torregrosamacia, R., Chromium(VI) removal with activated carbons. *Water Res.* **1995**, *29*, 2174-2180.
70. Aboutorabi, L.; Morsali, A.; Tahmasebi, E.; Buyukgungor, O., Metal-organic framework based on isonicotinate N-oxide for fast and highly efficient aqueous phase Cr(VI) adsorption. *Inorg. Chem.* **2016**, *55*, 5507-5513.